Eur. Phys. J. B **25**, 407–416 (2002)
DOI: 10.1140/epjb/e20020046

THE EUROPEAN PHYSICAL JOURNAL B
EDP Sciences

Low temperature dependence of the penetration depth in YBCO thin films revisited by mm wave transmission and surface impedance measurements

S. Djordjevic[1], E. Farber[2], G. Deutscher[2], N. Bontemps[1,a], O. Durand[3], and J.P. Contour[4]

[1] Laboratoire de Physique de la Matière Condensée, École Normale Supérieure, 24 rue Lhomond, 75231 Paris Cedex 05, France
[2] School of Physics and Astronomy, Raymond and Beverly Sackler Faculty of Exact Science, Tel Aviv University, Ramat Aviv 69978, Israel
[3] THALES Research and Technology, 91404 Orsay, France
[4] Unité Mixte de Physique CNRS/THALES, 91404 Orsay, France

Received 7 May 2001 and Received in final form 18 October 2001

Abstract. We report results obtained with two different experimental set-ups in state-of-the-art YBCO thin films as similar as possible, prepared by pulsed laser deposition on $LaAlO_3$ substrates: a surface impedance measurement on 4000 Å thick films using a parallel plate resonator (10 GHz), and a far infrared transmission (100–400 GHz) measurement which requires thinner (1000 Å) samples. The former measurement yields the temperature variation of the penetration depth $\lambda(T)$ and the real part of the conductivity, provided the absolute value of $\lambda(T)$ is known. The latter yields the imaginary part of the conductivity, hence the absolute value of the penetration depth, as well as its temperature dependence at the measuring frequency. Combining these two experiments, we establish a quasi-linear temperature variation of $\lambda(T)$, with a 2 Å K^{-1} low temperature slope, and a fairly large zero temperature value $\lambda(T=0)$=(1800±200) Å . The scattering rate of the quasi-particles calculated from a two-fluids model shows that the films compare to good quality single crystals, where twice a larger slope has been found. This surprising behavior is described in detail, including an in-depth structural analysis of the samples in order to evaluate their similarities. We find that the 10 GHz data obtained in the thickest films can be fitted to the dirty *d*-wave mode in the unitarity limit, with an extrapolated slope of 3 Å K^{-1}, but yield a scattering rate that is difficult to reconcile with the high T_c (92 K) of the films.

PACS. 74.25 Nf Response to electromagnetic fields (nuclear magnetic resonance, surface impedance, etc.) – 74.76 Bz High-T_c films – 78.66 -w Optical properties of specific thin films

1 Introduction

The linear temperature dependence of the low temperature penetration depth in the High T_c cuprates, first discovered by Hardy *et al.* in YBCO single crystals [1], has been one of the major advances in the understanding of these materials, as being fundamentally different from conventional superconductors. This linear dependence shows that in the cuprates, substantial excitations exist down to the lowest temperatures. Hardy *et al.* have interpreted their results in terms of a *d*-wave gap with lines of nodes, the linear temperature dependence of the penetration depth reflecting a linear density of states $N(E)$ at energies $k_BT \ll \Delta(0)$, where $\Delta(0)$ is the maximum gap. This interpretation was reported along with the fact that such a linear deviation from the $T = 0$ penetration depth $\Delta\lambda(T) = \lambda(T) - \lambda(0)$, was in agreement with the predictions of the *d*-wave theory: [2]

$$\Delta\lambda(T) = \frac{\ln(2)\lambda(0)}{\Delta(0)}T. \quad (1)$$

The slope $d\lambda/dT$ was measured in twinned single crystals and found to be (4.5±0.5) Å K^{-1}, up to 20 K [1,3,4]. Assuming $\lambda(0)$=1400 Å, this corresponds to $\Delta(0)$ of ∼20 meV, which is in agreement with the tunneling results [5].

Bonn *et al.* also reported that substitution by small amounts of Zn (0.3%) destroys the low temperature linear behavior whereas larger amounts of Ni appear harmless in this respect. These results, in particular in the case of Zn doping, were claimed to be in agreement with the predictions of the *d*-wave theory in the unitarity limit, with $\Delta\lambda \propto T^2$ at low temperatures. It could not be ascertained

[a] e-mail: nicole.bontemps@espci.fr

though, not knowing the absolute value of $\lambda(0)$ [6–9]. For compounds with a very small amount of scattering centers, the linear behavior is recovered beyond a cross over temperature T^*. An interpolation formula may be used in this latter case [7]:

$$\lambda(T) = \lambda(0) + \frac{bT^2}{T + T^*} \tag{2}$$

from which T^* and the actual linear slope b can be retrieved if T^* lies within the investigated temperature range.

Combining the measurement of $\Delta\lambda$ and that of the surface impedance, and assuming $\lambda(0)$=1450 Å, $\sigma_1(\omega, T)$ and the temperature dependence of the scattering rate was also calculated, using a two fluids model [10].

An alternative explanation for a linear dependence of $\Delta\lambda(T)$ was proposed by several authors [11–14] in terms of phase fluctuations of the order parameter, leading to the relation:

$$\Delta\lambda_f(T) \approx k_{\mathrm{B}}[8\pi\lambda^3(0)/\xi_0\phi_0^2]T \tag{3}$$

Taking $\lambda(0)$=1400 Å and the coherence length ξ_0=10 Å, this expression yields a slope $\mathrm{d}\lambda/\mathrm{d}T \cong 0.2$ Å K^{-1} much smaller than that found in single crystals. On that basis, this interpretation was discarded [15]. Comparing the expressions (1) and (3), we note that the value taken for $\lambda(0)$ has a much stronger influence on the fluctuation expression (Eq. (3)) than on the *d*-wave one (Eq. (1)). Therefore, in order to be able to discriminate between both models, it is necessary to gather the most relevant parameters, namely the temperature variation $\Delta\lambda(T)$ and the absolute value $\lambda(0)$. Also, as discussed at length further, the quasi-particle (QP) scattering rate $1/\tau$ is an important parameter since it results from the amount of scattering centers as well as from the strength of the potential (phase shift), and therefore implies a quantitatively different $\Delta\lambda(T)$ departure from the clean *d*-wave behavior.

In previous separate publications, we measured the temperature dependence of the penetration depth and of the surface impedance of state-of-the-art thin films using the parallel plate resonator technique (PPR) [16], and the frequency dependence of $\lambda(T, \omega)$ by mm wave transmission (mmT) through thinner films of similar quality [17]. The latter technique lends the absolute value of $\lambda(0)$, and an estimate of the scattering rate from the change of the temperature variation of $\lambda(T, \omega)$, but does not allow to calculate $\sigma_1(\omega, T)$. The PPR technique gave slopes of 2.2 Å K^{-1} for the best sample, while the mmT data were extrapolated to a zero frequency slope of 3.5 Å K^{-1}. The PPR result was definitely lower than that found in single crystals, but the transmission one could be compatible with it. In addition, a comparison between PPR results obtained in films of different quality suggested that the slope was smaller for better quality samples [16].

The two techniques being complementary, it was decided to repeat both sets of experiments on films that would be as similar as possible, and of the highest possible quality, in order to derive the absolute value of the penetration depth, and a cross estimate of the scattering rate. The results are presented in this paper. Section 1 reports on the detailed structural characteristics of the films, Sections 2 and 3 on the parallel plate and transmission results respectively; in Section 4, the two sets of data are compared and discussed; in Section 5, our new results are compared to previous ones, and tentative conclusions are drawn.

2 Samples preparation and characterization

2.1 Preparation

Films were prepared in situ by Pulsed Laser Deposition (PLD) in a multitarget LDM 32 Riber machine using a frequency tripled Nd:YAG laser (B.M. Industries 503 DNS) with a pulse length of 5 ns at a repetition rate from 1 to 5 Hz. It delivers a laser beam at 3550 Å wavelength with a power density from 50 to 600 MW/cm^2 depending on focusing the laser beam on the target. In this work, the growth parameters have been set in order to obtain a deposition rate at 2.6 Å s^{-1} for $YBa_2Cu_3O_7$ (YBCO) at a repetition rate of 2.5 Hz and a substrate-target distance of 35 mm. The YBCO target, which is stoichiometric with a density higher than 0.9 of the theoretical one, is continuously moved to ensure a uniform ablation rate. Before the growth, the (012) $LaAlO_3$ substrates are cleaned by heating in pure oxygen up to 800 °C for 10 min at a pressure of 40 Pa. After this cleaning procedure, cleanness and flatness of the surface are verified by RHEED before starting the growth procedure. The growth temperature was 785 °C measured at the surface of the substrate holder. The growth was carried out in 40 Pa pure oxygen pressure. During the deposition the substrate holder was continuously rotated at 45 rpm. At the end of the deposition, the pressure was increased to 4 10^4 Pa. Samples were then cooled down to room temperature within 45 min including an intermediate temperature plateau at 400 °C during 15 min.

2.2 Resistivity measurements

Resistivity is determined by an in-line four-point probe method [18], the calculated correction shape factor being verified by measurements performed on patterned lines in a YBCO film. The resistivity is linear, typical values at 300 K being 250 $\mu\Omega$ cm. The critical temperatures T_{c} – determined at zero resistance – are 92 K and 89 K for the 4000 Å and 1000 Å samples respectively. The transition widths are less than 0.5 K. The surface resistance (R_{s}) measurements which were carried out at 77 K and 10 GHz by the dielectric resonator method using titanium oxide (TiO_2) as dielectric. The diameter and the thickness of the resonator are respectively 7 and 1 mm, its dielectric constant is 105 with a loss coefficient of 1×10^{-5} at 77 K [19,20]. We measured R_{s}= 0.31 and 0.28 mΩ for the PPR films, and 1.03 mΩ for the thinner film used in the transmission measurement. The latter value is given without any thickness correction. Correcting for thickness would yield ∼0.5 mΩ.

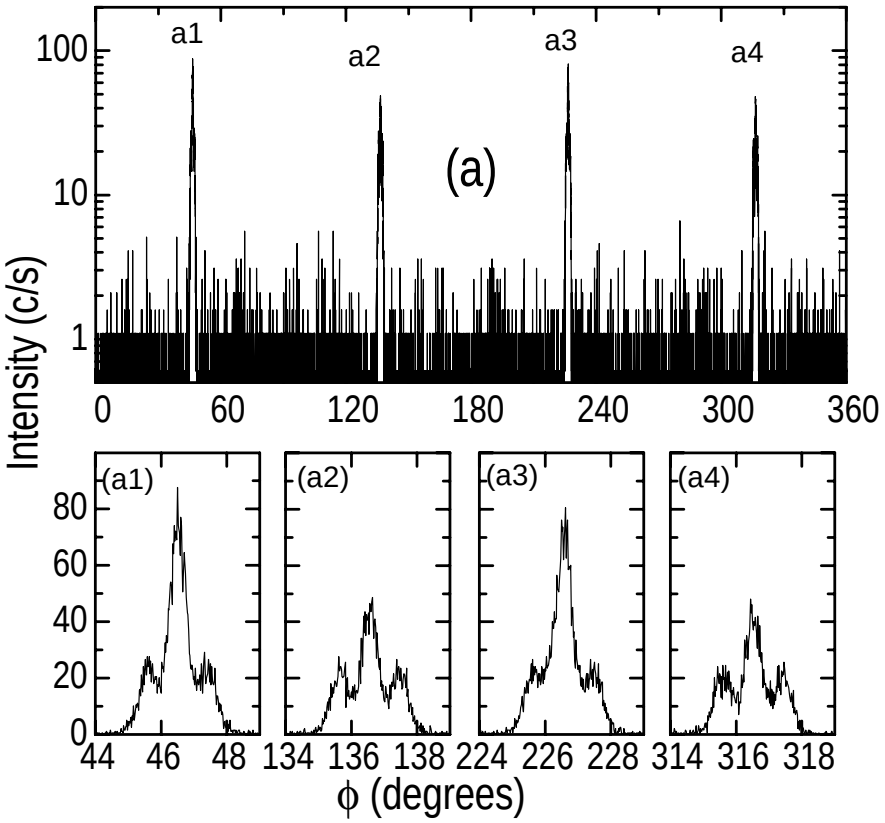

Fig. 1. (a) XRD Φ scans of the 1000 Å thick film. – and zooms (a1, a2, a3, a4) – on the $[2\bar{2}7]$ and [227] reflections.

Table 1. Summary of XRD Analysis. Samples are identified by the thickness. FWHM: Full Width at Half Maximum

Sample	4000 Å	1000 Å
Parameters (Å)	$a = 3.830$	$a = 3.829$
	$b = 3.896$	$b = 3.889$
	$c = 11.687$	$c = 11.699$
FWHM (005) (degree)	0.288	0.285
FWHM (102) (degree)	0.56/0.57	0.67/0.71
FWHM (227) (degree)	0.62/0.63	0.49/0.51
Twinning rate $\langle 110 \rangle$ (227)	0.56%/0.44%	61%/39%

2.3 XRD analysis of the $YBa_2Cu_3O_7$ films

Two types of YBCO films deposited both on (012) $LaAlO_3$ substrate, whose source is the same fabrication batch, have been studied: i) $\sim$ 1000 Å thick film for mm wave transmission measurements, ii) 4000 Å thick film for R_s measurements using PPR. The analysis has been carried out by using a Bragg-Brentano-geometry $\theta/2\theta$ and a 4-circle X-ray diffractometers with CuK_α sources with $\lambda(K_\alpha) = 1.54184$ Å. This XRD analysis was performed in order to determine to which extent such sets of samples are similar in a large range of thickness. The results are summarized in Table 1 and illustrated in Figure 1 (1000 Å sample) and Figure 2 (4000 Å sample).

No significant difference is observed in the $\theta/2\theta$ charts, which show that the films are purely c-axis oriented, the full widths at half maximum (FWHM) of the rocking curve of the (005) reflection being 0.285 and 0.288 degrees for the 1000 Å and 4000 Å thick films respectively. The ϕ-scan of the (101)/(011)/$(\bar{1}01)$/$(0\bar{1}1)$ reflections of the substrate and (102)/012/$(\bar{1}02)$/$(0\bar{1}2)$ reflections of the YBCO layer do not reveal any 45° orientation of the epitaxial layer with respect to the substrate axes. However, the FWHM of the (102) reflections is roughly constant and sharper (0.56–0.57°) for the 4000 Å thick film than for the 1000 Å one where it varies between 0.67 and 0.71° with respect to the ϕ angle. This broader FWHM indicates a slight increase in the misorientation of the epilayer around this axis with respect to the substrate.

The in-plane parameters have been determined from the chart of the (038)/(308) reflections, combined with the determination of the c-axis parameter from the $\theta/2\theta$ scans. A significant increase of the orthorhombicity of the YBCO cell is observed as the film thickness is increased from 1000 Å to 4000 Å, the $(b - a)$ value varying from (0.060±0.001) Å to (0.066±0.002) Å. Furthermore, the thinner film results are consistent with a marked residual compressive in-plane stress which is probably induced by the lattice mismatch between YBCO and $LaAlO_3$ ($\Delta_{aa}/a = -0.83\%$, $\Delta_{ab}/a = -2.6\%$), a corresponding tensile stress leading to a (0.012±0.004) Å expansion of the c parameter. This assumption is in good agreement with the results previously reported for YBCO films grown on $SrTiO_3$ and $NdGaO_3$ which have established that the deposition of a 3000 Å thick YBCO layer is necessary to eliminate the residual stress occurring in the epilayer above the limit of elastic accommodation [21,22]. Finally,

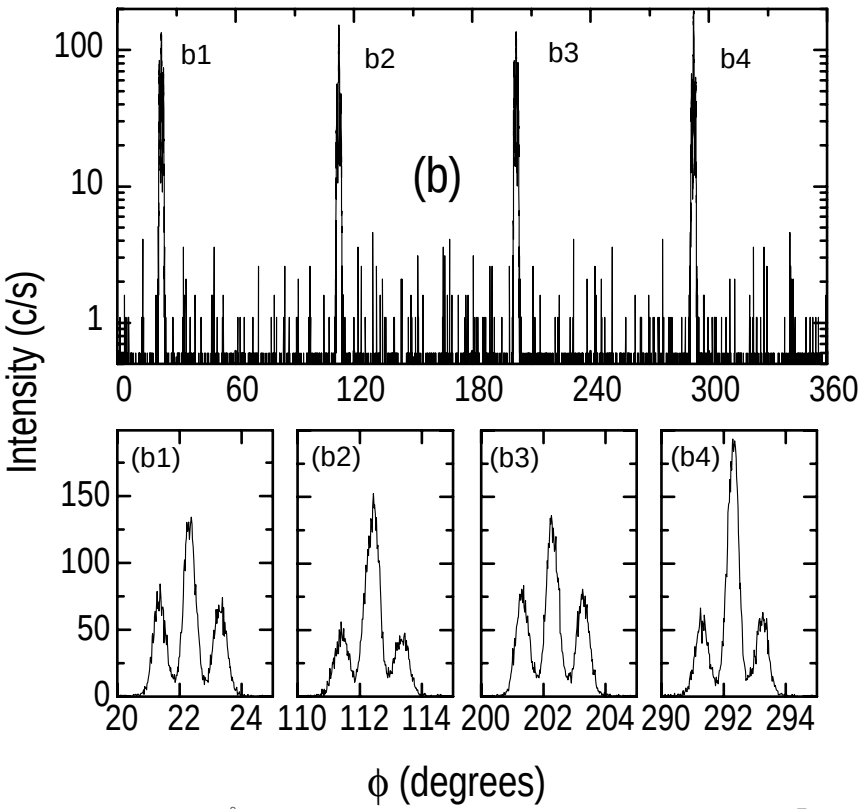

Fig. 2. (b) XRD Φ scans of the 4000 Å thick film – and zooms (b1, b2, b3, b4) – on the $[2\bar{2}7]$ and [227] reflections.

the ϕ-scan of the (227) reflections shows a twinning rate along the [110] and $[1\bar{1}0]$ directions more strongly asymmetric in the thinner film (61%/39%) than in the thicker one (56%/44%).

In summary, it can be concluded that, although the 1000 Å and the 4000 Å thick YBCO films present similar structural properties, the thinner one is slightly more disordered and shows a weak in-plane compressive epitaxial stress which decreases the b parameter of the YBCO cell while it expands its c-axis.

3 PPR measurements

In this section we present the experimental results of the 4000 Å YBCO thick films using the PPR method. In the PPR method one can deduce the surface resistance directly from the measured quality factor Q, and corrections are usually negligible [23]. The absolute value of λ cannot be measured by that method. But its change with temperature can be determined with a very high accuracy, because of the high Q value of the PPR for these films (typically of the order of 20 000): this yields a very high resolution in the penetration depth measurements, $\delta(\Delta\lambda) < 0.1$ Å. Such a high resolution on the change of the penetration depth can hardly be achieved by other cavity methods [1,24,25]. Details about the experimental technique have been given elsewhere [16]. In the present experiment, the PPR was operated using Teflon (FEP) as a dielectric spacer and was controlled by a vector network analyzer HP-8510c.

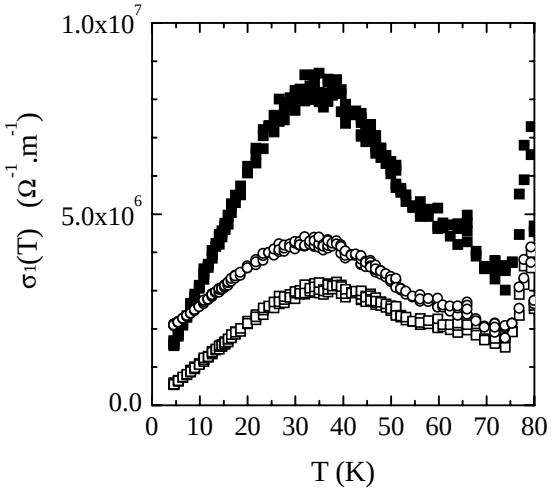

Fig. 3. Real part of the conductivity computed from PPR surface resistance data $R_s(T)$, after subtracting the residual surface $R_{res}(T = 0)$. Squares show $\sigma_1(T)$ when taking for the value of the penetration depth $\gamma(0) = 1300$ Å (full symbols) and 1800 Å (open symbols). Open circles show in the latter case the change in $\sigma_1(T)$ if $R_{res}(T = 0)$ is not subtracted.

The real part of the conductivity, *i.e.* $\sigma_1(T)$, is shown in Figure 3. It was obtained by using the relation $\sigma_1 \sim 2R_S/\lambda^3(\omega\mu_0)^2$ which holds as long as $\sigma_1 \ll \sigma_2$, a condition valid almost up to T_c [16]. We assumed $\lambda(0) = 1800$ Å, as determined by the FIR transmission method (see below). For the sake of comparison, we also show the result when using a lower bound value $\lambda(0)$=1300 Å (an average of the penetration depths measured by infrared spectroscopy in

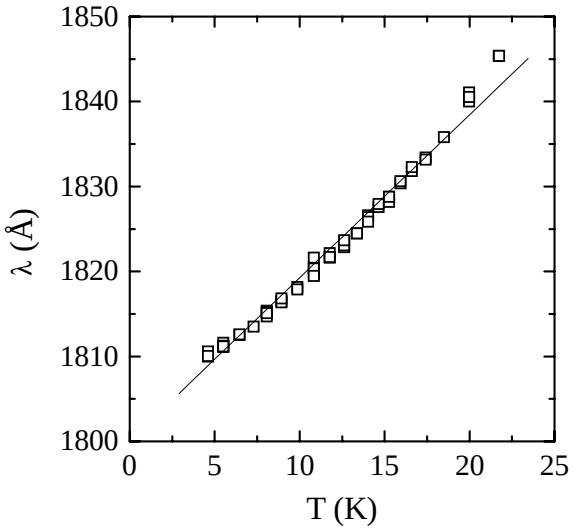

Fig. 4. Low temperature dependence of the penetration depth from PPR data. The solid line shows the best linear fit, yielding a slope of 2 Å K^{-1}.

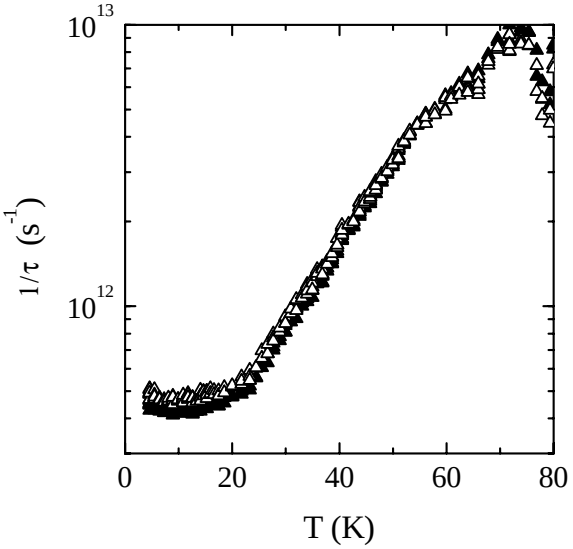

Fig. 5. Temperature dependence of the scattering rate deduced from the real part of the conductivity, in the framework of the two fluids model, after subtracting $R_{\rm res}(T = 0)$. The derivation has been performed using $\lambda(0) = 1300$ Å (full symbols) and $\lambda(0) = 1800$ Å (open symbols).

the a and b direction [26]), because we cannot rule out definitely the possibility (discussed in Sect. 4) that the thicker films being less disordered, $\lambda(0)$ measured in the thinner one may not be suitable for the thicker ones.

Two sets of curves are displayed in Figure 3: one set was calculated using the measured surface resistance $R_{\rm s}$, and the other after subtracting the extrapolated residual surface resistance $R_{\rm res}(T = 0) \cong 30$ $\mu\Omega$ at $T = 0$ K.

The *d*-wave theory predicts a finite conductivity at $T = 0$, $\sigma_{\rm min} = ne^2/m\pi\Delta(0)$, resulting in $R_{\rm min}(T = 0) \sim 1$ $\mu\Omega$ at 10 GHz. In our case, $R_{\rm res}(T = 0)$ is smaller than figures obtained by the same technique in other thin films [31]. It is of the same order of magnitude as in twinned single crystals [3,27–30] but indeed higher than the predicted *d*-wave value. Such small residual losses of our YBCO thin films and the distinct broad maximum around 40 K (much less sharp though than in single crystals), are good indications for the high quality of the samples. This non monotonic behavior of $\sigma_1(T)$ has been explained by a simple Drude analysis for the conductivity of unpaired carriers, assuming that their scattering time increases abruptly below $T_{\rm c}$, thus competing with the decrease of the density of uncondensed quasi-particles [3,10,28–30].

Figure 4 shows the variation of the penetration depth as a function of temperature at 10 GHz. The linear fit gives a slope of (2 ± 0.01) Å K^{-1} for $\lambda(0)$=1800 Å, and (2.2 ± 0.01) Å K^{-1} for $\lambda(0)$=1300 Å. The slight curvature may be an indication for the presence of imperfections in the films. It was argued that disorder due to clustering could explain the slight curvature also observed in high purity single crystals [32]. This curvature, in the latter report, disappears in samples which have both been detwinned and fully oxygenated. It may therefore be difficult to ascertain where this curvature comes from. This point will be further discussed in Section 5.

The scattering rate can be calculated in two different ways: either by subtracting the residual surface resistance $R_{\rm res}(T = 0)$ or from the raw data. We decided to subtract the $R_{\rm res}(T = 0)$ contribution. The result is shown in Figure 5. The scattering rate decreases abruptly below $T_{\rm c}$ and comes close to a constant value ∼5 10^{11} s^{-1} below 25 K. Our data are compatible with the values shown for YBCO single crystals by Bonn *et al.* [3].

4 Transmission measurements

In this part, we report on transmission measurements in the thinner film in the 130-400 GHz frequency range. The transmission set-up and the analysis of the data have been described in detail elsewhere [17,33]. Transmission measurements give access to the penetration depth, $\lambda(T)$ [17,33,34]. Transmission is indeed controlled by the complex conductivity $\sigma(\omega)$ which writes:

$$\sigma(\omega, T) = \sigma_1(\omega, T) - \frac{\rm i}{\mu_0 \omega \lambda^2(T)} \qquad (4)$$

in the superconducting state. It was verified [17] that the imaginary part of the conductivity is the dominant term at temperatures lower than 60 K. For sake of simplicity, we give now a simplified expression of the transmission t_n (normalized to the one at 110 K > $T_{\rm c}$)

$$t_n = \mu_0^2 \omega^2 \lambda^4(T) \sigma_n(110K) \qquad (5)$$

where σ_n(110K) is the conductivity at 110 K. This expression does not take into account the interference pattern

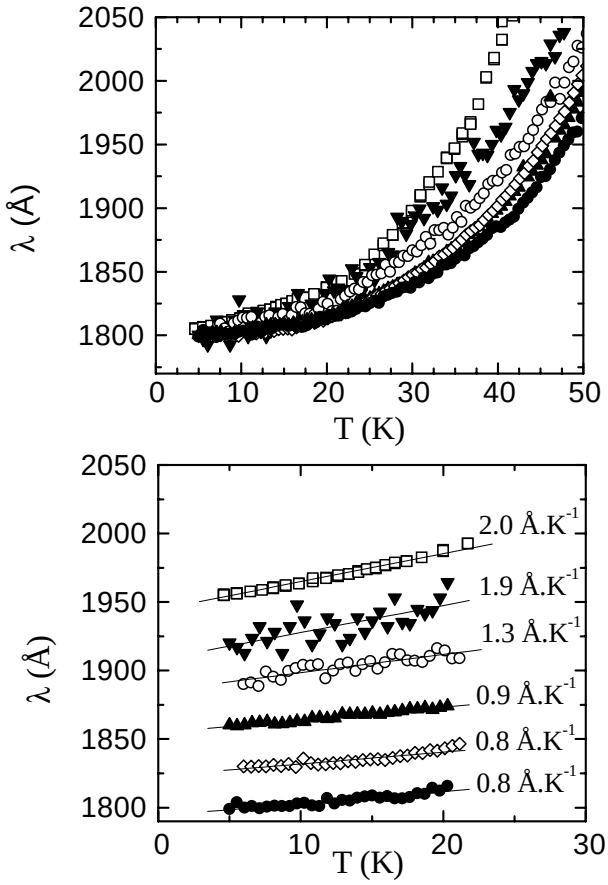

Fig. 6. Temperature dependence of the penetration depth from PPR and transmission data. Upper panel: 5–50 K temperature range. Lower panel: best linear fits up to 20 K, at the various frequencies. The data have been shifted by 30 Å, starting from the highest frequency. Note the gradual decrease of the slope as the measuring frequency increases. Symbols: 10 GHz, open squares; 134 GHz, full down triangles; 250 GHz, open circles; 333 GHz, full up triangles; 387 GHz, open diamonds; 400 GHz, full circles.

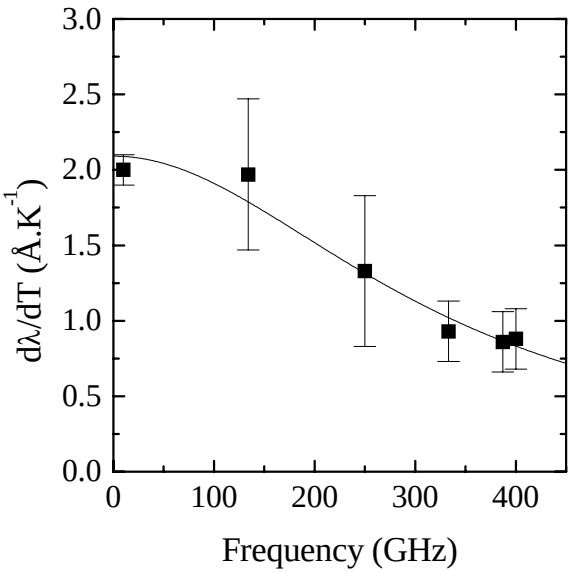

Fig. 7. Frequency dependence of the low temperature slope $\mathrm{d}\lambda/\mathrm{d}T$ obtained when fitting $\Delta\lambda(T)$ from both experiments to a straight line for $5 < T < 20$ K. The solid line shows the best fit to the two fluids variation assuming a frequency independent scattering rate (Eq. (6)), yielding $1/\tau = (2.1 \pm 0.1)\ 10^{12}\ \mathrm{s}^{-1}$.

through the substrate [35], however the results reported here have been analyzed using the complete expressions as explained in [17]. The transmission gives simultaneously the penetration depth temperature variation $\Delta\lambda(T)$ and its absolute value $\lambda(0)$. This determination requires the knowledge of the resistivity of the sample at 110 K, whose accuracy has been examined in detail. It was found, for all samples, that $\rho(110\mathrm{K})$ is 100 $\mu\Omega\,$cm within a 10% accuracy.

We have performed transmission measurements at five different frequencies 134, 250, 333, 387 and 400 GHz. For each frequency, we extract the corresponding temperature dependence of the penetration depth $\lambda(T)$. The upper panel of Figure 6 shows the penetration depth as a function of temperature for $T < 50$ K – including the PPR data. Each $\lambda(T)$ curve derived from transmission data at a given frequency, is an average over typically 5 to 10 measurements. The absolute value $\lambda(0)$ is estimated to be $\lambda(0) = (1800 \pm 200)$ Å.

The most striking feature is that the temperature dependence of the penetration depth $\lambda(T)$ becomes less and less pronounced as the frequency increases, meaning that we measure actually a frequency dependent penetration depth $\lambda(\omega, T)$. We assigned in our earlier work this behavior to the frequency becoming comparable to the scattering rate $1/\tau$, *e.g.* $\omega\tau \sim 1$ [17]. This interpretation can be understood in the framework of the two fluids model: as soon as the QP scattering rate $1/\tau$ is of the order of ω, the imaginary part of the conductivity involves a significant contribution of the normal fluid, which results into a smaller change of the temperature variation $\mathrm{d}\lambda/\mathrm{d}T$ as the frequency increases [36]. The frequency dependence has also been computed from the *d*-wave microwave conductivity in the limit $\omega \ll kT$ [9]. In the transmission measurement, our highest frequency corresponds to ~ 20 K, and therefore the latter calculation may not apply. The lower panel of Figure 6 focuses on the low temperature part ($5\mathrm{K} < T < 20$ K) of the $\lambda(T)$ data (the curves have been shifted by 30 Å for clarity, starting from the highest frequency). Within the accuracy of the measurements, the temperature dependence is linear in this temperature range, selected for the matter of the forthcoming comparison with single crystals data [1]. Linear fits allow the determination of the slope $\mathrm{d}\lambda/\mathrm{d}T$ for each frequency. We find that $\mathrm{d}\lambda/\mathrm{d}T$ changes from (1.9 ± 0.4) Å K^{-1} at 134 GHz, to (0.8 ± 0.15) Å K^{-1} at 400 GHz. Figure 7 shows the $\mathrm{d}\lambda/\mathrm{d}T$ data as a function of frequency. The error bars have been estimated from the reproducibility on several runs and do not take into account the standard deviation to the best fit which can be neglected.

Using the two fluids model, the slope $\mathrm{d}\lambda/\mathrm{d}T$ reads

$$\frac{\mathrm{d}\lambda}{\mathrm{d}T}(\omega,T)=\frac{\mathrm{d}\lambda}{\mathrm{d}T}(0,T)\frac{1}{1+\omega^2\tau^2} \quad (6)$$

from which we can extract both the value of the slope in the zero frequency limit and the scattering rate $1/\tau$. The best fit, including the 10 GHz point, is obtained for $\frac{\mathrm{d}\lambda}{\mathrm{d}T}(0,T) = (2.0 \pm 0.1)$ Å K^{-1} and $1/\tau = (2.1\pm0.1)10^{12}$ s^{-1}.

5 Discussion and comparison of the results from the two techniques

We now turn to the discussion and the comparison of the data described in Sections 2 and 3. The absolute value of $\lambda(0) = (1800 \pm 200)$ Å is larger than the one generally mentioned in the literature for single crystals: μSR yields $\lambda(0) = 1400$ Å for twinned crystals [38]. From IR measurements performed on detwinned crystals along the a and b directions, one can infer an "average" value $\lambda(0) = (\lambda_a + \lambda_b)/2 = 1200$–$1300$ Å [26,32]. In principle, our measurement should be compared to IR, which relates to the same underlying analysis of the conductivity, but for such a comparison it would be useful to know the accuracy of the IR determination [26]. Possible explanations for our somewhat larger value are:

i) Slightly deoxidized high quality thin films exhibit the same T_c and the same c-axis parameter [39].
ii) Surface effects (within the penetration depth) are different in single crystals and thin films. For instance, twins of the substrate may generate some roughness, hence increasing $\lambda(0)$. In order to achieve a significant increase, the size of surface defects should however be of the order of the penetration depth [40], which can hardly be the case for our thin films. Therefore, we rule out this possibility.
iii) The films are twinned, hence chains in different domains are disconnected, and the microwave and mm-wave measurement would only probe the a direction. In this case, one should then compare our $\lambda(0)$=1800 Å value to λ_a=1600 Å. Both values are then compatible within the error bars.
iv) The thinner film, where $\lambda(0)$ was measured, is slightly more disordered than the thicker ones (Sect. 1). This could result in an increase of the penetration depth with respect to the thicker ones, due to the increase of the penetration depth within the d-wave model, associated with an increasing scattering rate due to defects. Another issue is the occurrence of Josephson junction effects at slightly misoriented grain boundaries. We recall that one expects $\lambda_{\mathrm{eff}}^2 = \lambda^2 + \lambda_J^2$ where λ_{eff} is the effective penetration depth of the film and λ_J the Josephson depth, related to the critical Josephson current [41]. One can infer, from a possible increase of the penetration depth due to Josephson junctions at the grain boundaries, an order of magnitude of the critical current density if limited by such junctions. We find $\sim$2 10^7 A cm^{-2}, a figure which is not inconsistent with the 4.2 K critical current densities in good films.

Because points i) and iv) cannot be discarded, we have decided to analyze the results using two values, 1800 Å and 1300 Å (Fig. 3, Fig. 5).

We present now the two sets of analysis which have been performed in the thin and thick films. In the framework of the two-fluids model, and assuming a Drude behavior for the uncondensed carriers, we obtained at low temperature ($T \leq 20$ K) $1/\tau$=5×10^{11} s^{-1} from PPR (Fig. 5) and $1/\tau = (2.1 \pm 0.1)$ 10^{12} s^{-1} from the $\mathrm{d}\lambda/\mathrm{d}T$ slopes of both PPR and transmission measurements (Fig. 7).

There is no inconsistency between finding a good agreement for the frequency dependence of the slopes for both experiments, and different low temperature scattering rates. Indeed, whatever the scattering time, $\omega\tau$ is always negligible with respect to 1 at 10 GHz (at most 0.1), hence the slope $\mathrm{d}\lambda/\mathrm{d}T$ is not affected. In order to reconcile the different values for $1/\tau$, a step out of the Drude model is to release the standard assumption of a frequency independent scattering rate. This has been already suggested empirically following various experimental observations [29,41]. We discussed this point briefly in an earlier paper [43]. However, we cannot rule out the possibility that more disorder in the thin film, as described in Section 1, induces more effective elastic scattering on the associated defects (whatever they are), hence a larger scattering rate. We will therefore consider henceforward, for the sake of the comparison with earlier low frequency data, our low frequency scattering rate value of $\sim 5 \times 10^{11}$ s^{-1}.

6 General discussion

We wish to discuss at this point our data in comparison with the most relevant results in films and single crystals already reported in the literature. We restrict this discussion to YBCO close to optimal doping. Let us start by summarizing the large body of literature about the temperature dependence in thin films.

The early results of the temperature variation of the penetration depth in thin films were fitted with a T^2 dependence [44–48]. It may be noted that the range over which the T^2 dependence appears to fit the data is somewhat variable, up to 20 K [46], 30 K [48] or 40 K [45,47]. Later on, it appeared clearly that some films display a linear dependence up to 20 K [16,31,34,49] with slopes $\sim$ 4 to 5 Å K^{-1} or even larger (PPR measurement) [31,49] although in retrospect, the quality of these films could be questioned: some of them [31] exhibited a very large residual surface resistance which can be an indication of a large amount of defects. Another one [33], measured by transmission, did not display any frequency dependence, in contrast with the data reported above and in [17], a feature which can be understood as a consequence of a large scattering rate, hence again due to a significant amount of defects. Subsequently, with increasing reproducibility and control of the fabrication of thin films, surface reactance

measurements showed a quasi linear temperature dependence of the penetration depth at $T < 20$ K, however with a slope significantly lower than had been found before [16]. The results of [16] (2.2 and 3.8 Å K^{-1}) were incompatible with the single crystals results [3]. Also high frequency transmission measurements demonstrated a clear frequency effect of the temperature dependence of $\lambda(T)$ [17,50], which was assigned, in the same framework as described in Section 3, to the scattering rate being comparable to the measuring frequency. This suggested an increase of the QP life time in the superconducting state in these latter films with respect to the former ones (by roughly an order of magnitude). This interpretation was supported by the absence of any frequency effect in a purposely damaged sample [17].

It should be pointed out that a T^2 dependence must be considered with care as long as the value of the penetration depth is not known. It seems a reasonable starting point to discard films with very large penetration depths values (>2000 Å), suggesting extrinsic sources for field penetration (weak links, large angle grain boundaries) [34]. The latest results in the state-of-art thin films report an absolute value for $\lambda(0) \sim 1800$ Å [17,34,39].

Single crystals have exhibited a more stable behavior since 1993, when it was first shown that $\Delta\lambda$ exhibits a linear temperature dependence, with a slope of ~ 4 Å K^{-1} in twinned single crystals [1,4]. Although very recent measurements on YBCO single crystals grown in $BaZrO_3$ crucibles have raised a controversy [32,51] dealing with the temperature dependence up to T_c, the low temperature dependencies of $\lambda(T)$ are the same. Again, the dependence in twinned crystals close to optimal doping is quasi-linear up to 20 K with a value ~ 4 ÅK^{-1}, although a clear (if small) upward curvature is present. This curvature decreased when these crystals were detwinned and subsequently annealed in order to achieve over-doping [32], following a suggestion that at optimal doping oxygen atoms tend to cluster, hence to produce disorder [52].

Surface resistance was analyzed in early work in twinned crystals in the framework of a two fluids model, including a Drude behavior for QP, and yielded a drop of the scattering rate at low temperature, with respect to its normal state value, of two orders of magnitude down to $1/\tau \sim 2 \times 10^{11}$ s^{-1} [3,27]. Our results described in Section 2 and discussed in Section 4 show the same trend $1/\tau \sim 5 \times 10^{11}$ s^{-1}, whichever $\lambda(0)$ value is selected. Since our films are twinned (Sect. 1), we henceforth compare our data to that of twinned single crystals. As discussed at the beginning of this section, we cannot be sure that all samples to be compared (films and crystals) have the same oxygen doping level, although considering the critical temperature, it has to be very close. Despite these questions we nevertheless proceed with the comparison. The surface resistance shown in this work exhibits similar values in films as was found in single crystals. In particular, using the same analysis as Bonn *et al.* [3], the effective scattering rate is roughly the same in our thin films and in single crystals. Whether this analysis bears any meaning or not, we take this $1/\tau$ value as a parameter which may be used to compare one sample to another one. A clear increase of $1/\tau$, as impurities are added in crystals [2,26] or as films are damaged [17], is observed. Therefore retrieving the same $1/\tau$ at low frequency in different samples strongly suggests that the samples are of very similar quality.

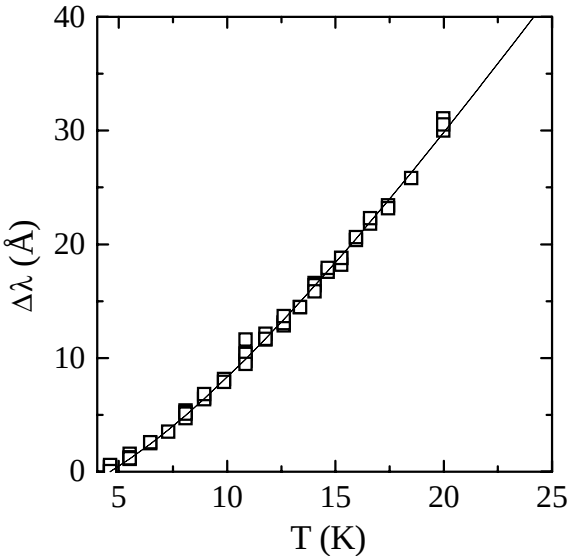

Fig. 8. Fit of the temperature variation $\Delta\lambda(T)$ of the penetration depth from PPR data to the interpolation formula (Eq. (2), assuming the *d*-wave model with resonant scattering.

We are then left with the conclusion that apparently similar films and single crystals, where T_c and $1/\tau$ exhibit close values, display a different temperature dependence of λ. The most striking observation is that the slopes differ by a factor of two between films and single crystals.

Disorder or the nature of defects have been argued to be relevant to explain the different behavior of films and crystals in the *d*-wave framework. We have therefore attempted to fit the 10 GHz data, which have the highest accuracy, to the interpolation formula (Eq. (2)). Such a procedure implies the assumption that there are in our films scatterers as strong as Zn, which is by no means obvious. Nevertheless, we show the results in Figure 8. The fit yields a cross over temperature T^*=16 K, with little dependence on the value selected for $\lambda(0)$: the intrinsic slope is (3.0 ± 0.1) Å K^{-1} for $\lambda(0) = 1800$ Å and (3.4 ± 0.1) Å K^{-1} for $\lambda(0) = 1300$ Å (Fig. 8 shows the fit for $\lambda(0)$= 1800 Å). These values look quite acceptable. To proceed further, since $T^* \approx 0.83\sqrt{\Gamma\Delta_0}$ [7], we may derive, for the sake of the comparison and using strictly the same procedure as in [7], the value of T^* in Zn doped YBCO single crystals with 0.15% ($\Gamma = 0.009$) and 0.31% Zn impurities ($\Gamma = 0.018$) respectively [9]. We find T^* values of 13 and 18 K respectively. The critical temperatures were in this case lowered from 93.4 K to 91.5 K and 89.5 K respectively. In our sample $T_c = 92$ K, whereas from the above comparison, we would expect T_c in between 91.5 and 89.5 K, presumably closer to 89.5 K. Moreover, $1/\tau$ in these Zn doped single crystals was found to saturate

at about 1.4×10^{12} s^{-1} [3] while in our films it achieves the significantly lower value of 5×10^{11} s^{-1}. Both observations suggest strongly that the *d*-wave model in the case of resonant scattering does not properly apply to our samples. Resonant scattering is only one particular limit, since it corresponds to a scattering phase shift $\delta = \pi/2$. Finite frequency effect and intermediate phase shifts have been considered, which yield a quasi-linear low temperature dependence of the penetration depth, with larger or smaller slopes, depending upon the value for δ [54]. The latter calculation being restricted typically to the range 0 to 14 K, a quantitative comparison remains to be done, in our temperature range, and using similar parameters.

Another physical explanation which might come into play, if we assume that the large value of $\lambda(0)$ describes correctly the thick films, are the phase fluctuations mentioned in the introduction. The role played by such fluctuations is increased by disorder. For instance, in clean single crystals where $\lambda(0)$ is believed to be of the order of ~ 1400 Å, the linear temperature variation of the penetration depth $\Delta\lambda_{\rm f}(T)$ due to fluctuations is negligible: $\Delta\lambda_{\rm f}(T) \sim 0.2$ Å K^{-1}. Thin films may be more disordered than single crystals, in which case $\lambda(0)$ is increased (in the *d*-wave scenario). Interestingly, if $\lambda(0)$ achieves values of the order of 1800 Å, as we measured, then $\Delta\lambda_{\rm f}(T) \sim 1.4$ Å K^{-1}, which, considering the crudeness of the approximations gives a value fairly close to our value of 2 Å K^{-1} without any adjustable parameters.

In conclusion, we have performed a thorough study of state-of-the-art thin films, using complementary techniques which also allow to cross-check the values that are derived, in particular the scattering rate. On one hand, our data for the penetration depth can be interpreted within the standard *d*-wave model, including resonant scattering with a small amount of unknown impurities or defects, yielding a slight curvature of the temperature dependence of $\Delta\lambda(T)$ at low frequency (thanks to the very high resolution of the PPR experiment). The slope of the linear part is then found to be in the range of 3.0 Å K^{-1} to 3.5 Å K^{-1}, and the crossover temperature between the quadratic and the linear part is $T^* \sim$16 K. This behavior may look similar to that of Zn doped single crystals. But we stress that our films have a higher $T_{\rm c}$ and a lower scattering rate than these crystals. Our complete data set is therefore not easily understood within the *d*-wave theory by including resonant scattering; an intermediate phase shift might describe more correctly the data; this remains to be worked out. On the other hand, considering the value of $\lambda(0)$ measured in the thinner films, the contribution of phase fluctuations would be much closer to our measured low temperature slope, hence their contribution cannot be ruled out.

The authors wish to thank E. Jacquet and S. Berger for their helpful contributions in thin films elaboration and resistivity measurements. They are also grateful to B. Marcilhac and Y. Lemaître for helpful discussions and assistance in surface resistance measurements.

References

1. W.N. Hardy, D.A. Bonn, D.C. Morgan, Ruixing Liang, Phys. Rev. Lett. **70**, 3999 (1993).
2. D.J. Scalapino, Physics Rep. **250**, 239 (1995).
3. D.A. Bonn *et al.*, Phys. Rev. B **50**, 4051 (1994).
4. J. Mao *et al.*, Phys. Rev. B **51**, 3316 (1995).
5. B.A. Aminov *et al.*, J. Supercond. **7**, 361 (1994).
6. H. Kim, G. Preosti, P. Muzikar, Phys. Rev. B **49**, 3544 (1994).
7. P.J. Hirschfeld, N. Goldenfeld, Phys. Rev. B **48**, 4219 (1993).
8. P.J. Hirschfeld, W.O. Putikka, D.J. Scalapino, Phys. Rev. Lett. **71**, 3705 (1993).
9. P.J. Hirschfeld, W.O. Putikka, D.J. Scalapino, Phys. Rev. B **50**, 10250 (1994).
10. D.A. Bonn *et al.*, Phys. Rev. B **47**, 11314 (1993).
11. E. Roddick, D. Stroud, Phys. Rev. Lett. **74**, 1430 (1995).
12. M.W. Coffey, Phys. Lett. A **200**, 195 (1995).
13. V.J. Emery, S.A. Kivelson, Phys. Rev. Lett. **74**, 3253 (1995).
14. V.J. Emery, S.A. Kivelson, Nature **374**, 434 (1995).
15. T.R. Lemberger *et al.*, *Proceedings SPIE Oxide Superconductor Physics and Nanoengineering II*, **2697**, 211 (1996).
16. E. Farber, G. Deutscher, J.P. Contour, E. Jerby, Eur. Phys. J. B **5**, 159 (1998).
17. S. Djordjevic, L.A. de Vaulchier, N. Bontemps, J.P. Vieren, Y. Guldner, S. Moffat, J. Preston, X. Castel, M. Guilloux-Viry, A. Perrin, Eur. Phys. J. B **5**, 847 (1998).
18. E.M. Smits, Bell Syst. Techn. J. May, 714 (1958).
19. Y. Lemaître, L.M. Mercandalli, B. Dessertenne, D. Mansart, B. Marcilhac, J.C. Mage, Physica C **643**, 235–240 (1994).
20. J.C. Mage, J. Dieumegard, *AGARD Conf. Proceedings*, **481**, 104 (1990).
21. M. Ece, E. Garcia-Gonzales, H.U. Habermeier, J. Appl. Phys. **77**, 1646 (1995).
22. J.P. Contour, A. Abert, A. Défossez, *SPIE Proceedings*, **2697**, 339 (1996).
23. R.C. Taber, Rev. Sci. Instrum. **61**, 2200 (1990).
24. H. Walter *et al.*, Phys. Rev. Lett. **80**, 3598 (1998).
25. H. Srikanth *et al.*, Phys. Rev. B **55**, R14733 (1997).
26. D.N. Basov *et al.*, Phys. Rev. Lett. **74**, 598 (1995).
27. D.A. Bonn *et al.*, Czech. J. Physics **46** Suppl. **S6**, 3195 (1996).
28. D.A. Bonn, W.N. Hardy, *Physical Properties of High Temperature Superconductors*, Vol. 7, edited by D. Ginsberg (World Scientific Publishing, 1996).
29. T. Shibauchi *et al.*, Physica C **203**, 315 (1992). T. Shibauchi *et al.*, J. Phys. Soc. Jpn **65**, 3266 (1996).
30. D.A. Bonn, J. Phys. Chem. Solids **54**, 1297 (1993).
31. E. Farber, G. Deutscher, G. Koren, E. Jerby, *Nineteenth IEEE convention* (Israel, 1996).
32. S. Kamal *et al.*, Phys. Rev. B **58**, R8933 (1998).
33. L.A. de Vaulchier *et al.*, Phys. Rev. B **52**, 564 (1995).
34. L.A. de Vaulchier *et al.*, Europhys. Lett. **33**, 153 (1996).
35. R.E. Glover, M. Tinkham, Phys. Rev. **108**, 243 (1957).
36. N. Bontemps, L.A. de Vaulchier, R. Combescot, Ferroelectrics **177**, 127 (1996).
37. A. Hosseini *et al.*, Phys. Rev. B **60**, 1349 (1999).
38. J.E. Sonier *et al.*, Phys. Rev. Lett. **72**, 744 (1994).
39. A. Fuchs, W. Prusseit, P. Berberich, H. Kinder, Phys. Rev. **53**, R14745 (1996).

40. F.F Mende, A.I. Spitsyn, N. Podlesnyi, Sov. Phys. Tech. Phys. **26**, 1512 (1981).
41. T.L. Hylton, M.R. Beasley, Appl. Phys. Lett. **53**, 1343 (1988).
42. A. Frenkel *et al.*, Phys. Rev. B **54**, 1355 (1996).
43. E. Farber *et al.*, J. Low Temp. Phys. **117**, 515 (1999).
44. J. Anett, N. Goldenfeld, S.R. Reno, Phys. Rev. B **43**, 2778 (1991).
45. A. Porch *et al.*, *Proceedings of the Applied Superconductivity Conference*, IEEE Trans. Appl. Supercond. **5**, 1987 (1995).
46. Zhengziang Ma *et al.*, Phys. Rev. Lett. **71**, 781 (1993).
47. H.E. Porteanu *et al.*, Phys. Rev. Lett. **75**, 3934 (1995).
48. J.B. Feenstra *et al.*, Physica C **278**, 213 (1997).
49. E. Farber, J.P. Contour, G. Deutscher, Physica C **317-318**, 550 (1999).
50. U. Dahne *et al.*, J. Supercon. **8**, 129 (1995).
51. H. Srikanth *et al.*, Phys. Rev. B **55**, 14733 (1997).
52. A. Erb *et al.*, J. Low. Temp. Phys. **105**, 1023 (1996).
53. Kuan Zhang *et al.*, Appl. Phys. Lett. **62**, 3019 (1993).
54. S. Hensen, G. Müller, C.T. Rieck, K. Scharnberg, Phys. Rev. B **56**, 6237 (1997).